Molecular Biology of the Cell
Vol. 21, 1282–1292, April 1, 2010

Manganese-induced Trafficking and Turnover of the *cis*-Golgi Glycoprotein GPP130

Somshuvra Mukhopadhyay,* Collin Bachert,* Donald R. Smith,† and Adam D. Linstedt*

*Department of Biological Sciences, Carnegie Mellon University, Pittsburgh, PA 15213; and †Department of Microbiology and Environmental Toxicology, University of California at Santa Cruz, Santa Cruz, CA 95064

Submitted December 1, 2009; Revised January 20, 2010; Accepted January 21, 2010
Monitoring Editor: Keith E. Mostov

Manganese is an essential element that is also neurotoxic at elevated exposure. However, mechanisms regulating Mn homeostasis in mammalian cells are largely unknown. Because increases in cytosolic Mn induce rapid changes in the localization of proteins involved in regulating intracellular Mn concentrations in yeast, we were intrigued to discover that low concentrations of extracellular Mn induced rapid redistribution of the mammalian *cis*-Golgi glycoprotein Golgi phosphoprotein of 130 kDa (GPP130) to multivesicular bodies. GPP130 was subsequently degraded in lysosomes. The Mn-induced trafficking of GPP130 occurred from the Golgi via a Rab-7–dependent pathway and did not require its transit through the plasma membrane or early endosomes. Although the cytoplasmic domain of GPP130 was dispensable for its ability to respond to Mn, its lumenal stem domain was required and it had to be targeted to the *cis*-Golgi for the Mn response to occur. Remarkably, the stem domain was sufficient to confer Mn sensitivity to another *cis*-Golgi protein. Our results identify the stem domain of GPP130 as a novel Mn sensor in the Golgi lumen of mammalian cells.

INTRODUCTION

The subcellular levels of ions and other micronutrients such as amino acids are closely regulated in eukaryotic cells. Alterations in the levels of these small molecules often induce rapid changes in the intracellular localization of proteins involved in regulating their subcellular concentrations. High levels of Cu lead to the translocation of the Cu-transporting pumps ATP7A and ATP7B from the *trans*-Golgi network (TGN) to the plasma membrane where they pump Cu out of the cell (La Fontaine and Mercer, 2007) and an autosomal recessive mutation in ATP7B gives rise to cellular copper accumulation and Wilson's disease (Kitzberger *et al*., 2005). In yeast, under conditions of amino acid excess, the general amino acid permease GAP1 is both endocytosed and degraded from the plasma membrane, and newly synthesized GAP1 transiting the Golgi is diverted to the vacuole for degradation without reaching the cell surface at all (Scott *et al*., 2004; Risinger and Kaiser, 2008). The yeast ferrichrome receptor ARN1, in contrast, is up-regulated in the presence of its substrate. In the absence of ferrichrome, ARN1 is targeted for degradation from the TGN to the vacuole (Deng *et al*., 2009). When low concentrations of ferrichrome are present in the medium, small amounts of it get internalized by fluid phase endocytosis and bind a high-affinity receptor domain in ARN1. ARN1 bound to ferrichrome traffics to the plasma membrane from the TGN, instead of the vacuole, where it rapidly pumps ferrichrome into the cell (Deng *et al*., 2009).

Regulation of the intracellular levels of Mn is particularly important. Mn is an essential cofactor required for the catalytic activity of diverse enzymes such as DNA and RNA polymerases, mitochondrial superoxide dismutases, Golgi enzymes required for *N*-linked glycosylation as well as certain decarboxylases and kinases (Missiaen *et al*., 2004). In the CNS, the majority of cellular Mn occurs as a cofactor in the astrocyte enzyme glutamine synthetase (Aschner *et al*., 1999). Although Mn is required in diverse cellular processes, exposure to high doses of Mn is toxic. In humans, over exposure to Mn results in the development of a Parkinson-like syndrome called manganism in occupationally exposed individuals (Olanow, 2004), whereas environmental exposure to Mn has been associated with cognitive and behavioral effects in children (Wright *et al*., 2006; Bouchard *et al*., 2007). Unlike Parkinson's disease, there is no medical management to treat or control the onset and progression of manganism (Olanow, 2004). Thus, elucidating the subcellular mechanisms that regulate Mn homeostasis and mediate its cytotoxic effects is of high clinical significance.

Studies of Mn homeostasis in yeast indicate the importance of regulated intracellular trafficking of Mn transporters. Smf1p, which is a member of the natural resistance-associated macrophage protein (NRamp) family of metal transporters, pumps extracellular Mn into the yeast cytosol (Culotta *et al*., 2005). Pmr1p, a P-type Ca- and Mn-transporting ATPase, then pumps cytosolic Mn into the lumen of the Golgi for use by enzymes of the glycosylation pathway. Under normal conditions, intracellular levels of Mn are regulated by adjustment of surface levels of Smf1p through endocytosis and ubiquitin-mediated targeting to the vacuole for degradation (Culotta *et al*., 2005). At toxic Mn levels,

This article was published online ahead of print in *MBoC in Press* (http://www.molbiolcell.org/cgi/doi/10.1091/mbc.E09–11–0985) on February 3, 2010.

Address correspondence to: Adam D. Linstedt (linstedt@andrew.cmu.edu).

Abbreviations used: Dyn, dynamin; EE, early endosome; EEA, early endosome antigen; GFP, green fluorescent protein; GPP130, Golgi phosphoprotein of 130 kDa; GP73, Golgi phosphoprotein of 73 kDa; Lamp, lysosome-associated membrane protein; MVB, multivesicular body; TGN, *trans*-Golgi Network; WT, wild type.

newly synthesized Smf1p protein transiting the Golgi is also diverted to the vacuole for degradation (Jensen *et al*., 2009) but Pho84p, an P_i transporter with low affinity for Mn, persists on the surface and pumps large amounts of Mn into the cytosol as metal-phosphate complexes (Culotta *et al*., 2005). The excess cytosolic Mn is removed as Pmr1p pumps it into the Golgi so that it will be secreted (Culotta *et al*., 2005). In addition, some cytosolic Mn may be sequestered in the yeast vacuole as a putative Mn pump has been identified in the vacuole and its loss leads to enhanced sensitivity to Mn (Gitler *et al*., 2009).

In mammals, mechanisms of Mn homeostasis and toxicity are not well understood. Multiple transporters mediate intracellular Mn uptake including splice isoforms of divalent metal transporter (DMT)1, which is a homologue of yeast Smf1p, the solute-carrier 39 metal transporter member ZIP8, transferrin receptor, various calcium channels, and the glutamate ionotropic receptor (Au *et al*., 2008). Some of these transporters are localized to intracellular compartments, such as DMT1 in lysosomes (Tabuchi *et al*., 2000), but it is not known whether increased Mn exposure alters their localization. Surprisingly, none of these transporters are specific for Mn and even the relative contribution of each transporter to the overall extent of uptake is not known (Au *et al*., 2008). Moreover, although the human homologue of the Golgi localized yeast Pmr1p pump secretory pathway Ca ATPase 1 (SPCA1) has been cloned (Sudbrak *et al*., 2000), its role in Mn detoxification, if any, has not been established (Missiaen *et al*., 2004). Additionally, while exposure to elevated levels of Mn enhances oxidative stress, induces apoptosis, fragments the Golgi apparatus, compromises mitochondrial function, changes cell cycle progression and increases production of mediators of inflammation like prostaglandins in mammalian cells in culture (Towler *et al*., 2000; Roth *et al*., 2002; Zhao *et al*., 2008; Milatovic *et al*., 2009), the molecular mechanisms by which elevated Mn causes cytotoxicity are still not well understood.

Here, we report that Mn induces the rapid trafficking of the *cis*-Golgi glycoprotein Golgi phosphoprotein of 130 kDa (GPP130) to multivesicular bodies (MVBs) with its subsequent degradation in lysosomes. GPP130 is an integral membrane protein with a large lumenal domain (Linstedt *et al*., 1997). The protein cycles within the Golgi and from the Golgi to endosomes (Bachert *et al*., 2001) and GPP130 depletion interferes with endosome to Golgi retrieval of specific proteins that traffic in the bypass pathway (Natarajan and Linstedt, 2004). Our studies define the pathway of Mn-induced redistribution of GPP130 and identify the GPP130 *cis*-acting elements necessary and sufficient for the response.

MATERIALS AND METHODS

Cell Culture and Transfections

HeLa cells were grown in minimum essential medium (MEM) with 100 IU/ml penicillin-G and 100 μg/ml streptomycin (Fisher Scientific, Hanover Park, IL) supplemented with 10% fetal bovine serum (Atlanta Biologicals, Lawrenceville, GA). For Mn treatment, freshly prepared $MnCl_2$ (Fisher Scientific) was added for the times and concentrations described in individual figures. DNA transfections were performed using the JetPEI transfection reagent (Genesee Scientific, San Diego, CA) according to the manufacturer's protocol. Cultures were routinely transfected 24 h after plating and used for experiments 24 h after transfection. RNA transfections were performed using the Oligofectamine transfection reagent (Invitrogen, Carlsbad, CA) according to the manufacturer's protocol. The small interfering RNA (siRNA) used targeted the sequence AAAAGCCAACACGAGGAGCTA in GPP130 cDNA and has been described previously by us (Natarajan and Linstedt, 2004). In the gene replacement experiments (Puthenveedu and Linstedt, 2004), cells were transfected with the replacement GPP130 construct 48 h after siRNA transfection by using JetPEI as described above. The replacement constructs had three silent mutations in the sequence targeted by the siRNA. These silent mutations were introduced using the forward primer 5′-CATCAGATGTTGAAAAGCCAACATGAAGAGCTCAAGAAA CAGCACAGTG-3′ and the QuikChange mutagenesis kit (Stratagene, La Jolla, CA). The mutated base pairs in the replacement construct are underlined.

Constructs

A fragment of GPP130 extending from amino acids 1-435 was nondirectionally cloned into the Hind-3 site of the pEGFP-N3 vector (enhanced green fluorescent protein) (Clontech, Mountain View, CA). This construct ($GPP130_{1\text{-}435}$-GFP) was used to create a deletion construct which had residues 1-247 of GPP130 ($GPP130_{1\text{-}247}$-GFP) using a polymerase chain reaction (PCR)-based loop-out modification of the QuikChange protocol. Further deletions were created using the $GPP130_{1\text{-}247}$-GFP construct. The deletion constructs created were as follows: $GPP130_{\Delta 176\text{-}247}$-GFP, $GPP130_{\Delta 88\text{-}247}$-GFP, $GPP130_{\Delta 36\text{-}175}$-GFP, $GPP130_{\Delta 36\text{-}87}$-GFP, $GPP130_{\Delta 88\text{-}175}$-GFP, and $GPP130_{\Delta 2\text{-}11}$-GFP. For chimeric Golgi phosphoprotein of 73 kDa (GP73)-GPP130 constructs, a fragment of GP73 extending from amino acid 1-184 (the end of its predicted coiled-coil stem domain) was inserted upstream of $GPP130_{1\text{-}247}$ between the Nhe1 and Xho1 sites of pEGFP-N3. The cytoplasmic and transmembrane domains of GPP130 (amino acids 1-35 of GPP130) were then deleted to obtain proper membrane topology. This construct was G73-$G130_{36\text{-}247}$-GFP. Further deletions in the GPP130 domains in the chimeric constructs were subsequently performed as described for the parent $GPP130_{1\text{-}247}$-GFP above to obtain G73-$G130_{36\text{-}175}$-GFP, G73-$G130_{88\text{-}247}$-GFP, G73-$G130_{176\text{-}247}$-GFP, G73-$G130_{36\text{-}87}$-GFP, G73-$G130_{88\text{-}175}$-GFP, and G73-$G130_{36\text{-}87\_176\text{-}247}$-GFP. For the chimeras, the amino acids of GPP130 present in the construct are expressed in their respective names. GFP-tagged Rab5 wild-type (WT), Rab5 S34N and Rab5 Q79L were from Allan Levey, Emory University, Atlanta, GA (Volpicelli *et al*., 2001);GFP-tagged Rab7 WT, Rab7 T22N, and Rab7 Q67L were from Marlyn Farquhar (University of California at San Deigo, La Jolla, CA) and have been described previously (Bucci *et al*., 2000), whereas hemagglutinin (HA)-tagged dynamin (Dyn) II WT and Dyn II K44A were from Sandra Schmid (The Scripps Institute, La Jolla, CA) (Damke *et al*., 1994). The GFP tag was removed from the Rab5 Q79L construct by the loop out technique described above.

Epidermal Growth Factor (EGF) Uptake and Degradation Assays

The EGF uptake and degradation assay was performed as described previously (Raiborg *et al*., 2001, Kauppi *et al*., 2002). In brief, cells were transferred to MEM containing 2% bovine serum albumin (BSA). Alexa Fluor 555-EGF complex (Invitrogen) was used at a final concentration of 200 ng/ml. For the uptake experiments, cells were loaded with EGF for 15 min at 37°C and then fixed with 3% paraformaldehyde (PFA) and processed for immunofluorescence microscopy. For the degradation assays, cells were loaded with EGF for 60 min at 37°C, then washed and chased for a further 60 min at 37°C in EGF-free medium. At the end of the chase, cells were permeabilized using phosphate-buffered saline (PBS) containing 0.03% saponin and 2% BSA at room temperature for 5 min. The Alexa Fluor dye is not degraded by lysosomal hydrolases and persists even after EGF itself is degraded. The saponin permeabilization before fixation releases the free Alexa tag from the cell without affecting undegraded Alexa Fluor-EGF complexes. After permeabilization, cells were fixed with 3% PFA and mounted for microscopy (Raiborg *et al*., 2001, Kauppi *et al*., 2002).

Immunofluorescence Microscopy

Cells were fixed with 3% PFA and immunofluorescence analyses was performed essentially as described previously (Yadav *et al*., 2008; Sengupta *et al*., 2009). Alexa Fluor 488-, Alexa Fluor 594-, Alexa Fluor 568-, or Cy5-tagged secondary antibodies were used (Invitrogen). Images were captured using a spinning-disk confocal scan head microscope equipped with three-line laser and independent excitation and emission filter wheels (PerkinElmer Life and Analytical Sciences, Boston, MA) and a 12-bit Orca ER digital camera (Hamamatsu Photonics, Bridgewater, NJ) mounted on an Axiovert 200 microscope with a 100×, 1.4 numerical aperture oil immersion objective (Carl Zeiss, Thornwood, NY). Sections at 0.5-μm spacing were acquired using Imaging Suite software (PerkinElmer Life and Analytical Sciences). All qualitative images depicted in the figures are maximum value projections of the collapsed Z-stacks.

Image Analyses

Immunofluorescence images were analyzed using ImageJ (http://rsbweb.nih.gov/ij). To measure fluorescence per cell, average value projections were created from individual Z-stacks, and background was subtracted from each image separately. The mean fluorescence per cell was calculated by drawing the outline of the cell and using the Analyze Measure function in ImageJ. To measure total number of endosomes per cell, maximum value projections were created, and the projected images were uniformly thresholded after background subtraction. Total numbers of cytoplasmic objects ranging between 10 and 100 pixels were calculated per cell using the Analyze Particle function of ImageJ. Line profiles were obtained using the RGB Profiler, and Pearson's coefficients were calculated using the Intensity Correlation Analysis

plug-ins of ImageJ, respectively. All quantitative fluorescence data are from a single experiment, and all experiments have been replicated at least three times, independently.

Viability Assays

The methylthiazolyldiphenyl-tetrazolium bromide (MTT) assay for cell viability was performed as described previously (Denizot and Lang, 1986; Zhao *et al*., 2008). HeLa cells were exposed to 0–16 mM Mn for 12 h, washed with PBS, and adjusted to 0.05% MTT (wt/vol, EMD Chemicals, Inc., Gibbstown, NJ) in PBS for 2 h at 37°C. Cells were then lysed using 500 μl of 0.1 N hydrochloric acid in isopropanol and 1% Triton X-100. Absorption was subsequently measured at 570 nm. Annexin-V-fluorescein isothiocyanate (FITC) (Sigma-Aldrich, St. Louis, MO) was used as described by the manufacturer. HeLa cells were treated with 500 μM $MnCl_2$ for 0–24 h. Subsequently, cells were incubated with Annexin-V-FITC used at a final dilution of 1:100 in buffer containing 100 mM HEPES/NaOH, pH 7.5, 1.4 M NaCl, and 25 mM $CaCl_2$ for 15 min at room temperature and mounted immediately for microscopy.

Immunoblot Analyses

For immunoblot assays cells were harvested in Tris-SDS lysis buffer (25 mM Tris-Cl, pH 6.7, 1.5% SDS, 0.8% β-mercaptoethanol, 1 mM dithiothreitol, and 1 mM polymethyl sulfonyl fluoride). Immunoblotting was performed as described previously (Yadav *et al*., 2008; Sengupta *et al*., 2009). Immunoblots were quantitated using ImageGauge software (Fujifilm, Valhalla, NY).

Antibodies and Other Reagents

Polyclonal (pAb) and monoclonal (mAb) antibodies against GPP130 and anti-HA mAb have been described previously (Linstedt *et al*., 1997; Puri *et al*., 2002). Unless indicated, all experiments used the anti-GPP130 pAb. The anti-GPP130 mAb binds GPP130 between amino acids 278-433 (Linstedt *et al*., 1997) and did not recognize any of the exogenously expressed GFP-tagged constructs used in this study. Monoclonal antibodies against early endosome antigen (EEA)1, α tubulin, and lysosome-associated membrane protein (Lamp)2 were from BD Biosciences (San Jose, CA), Sigma-Aldrich, and Abcam (Cambridge, MA), respectively. All chemicals were from Sigma-Aldrich unless otherwise specified.

Statistical Analyses

Comparisons between any two groups were performed using two-tailed Student's *t* test assuming equal variances. For comparing multiple groups at the same time, single-factor analysis of variance with the Tukey–Kramer post hoc test was used (NCSS 2007 software; NCSS, Kaysville, UT). An asterisk in bar graphs indicates $p < 0.05$.

RESULTS

The cis-Golgi Glycoprotein GPP130 Is Rapidly and Specifically Degraded in Response to Mn

In a test of the cellular response to 500 μM Mn, we observed that GPP130 levels were significantly reduced during an 8-h time course (Figure 1A). During the same period, the levels of a related *cis*-Golgi protein, GP73 (Puri *et al*., 2002), and the loading control tubulin were unaffected. Quantification indicated that GPP130 loss exceeded 65% at the 8-h time point (Figure 1B). In accordance with a previous report (Zhao *et al*., 2008), cell viability analyzed using the MTT assay and Annexin-V staining was unaffected during this period (data not shown). Specific loss of GPP130 was also confirmed by immunofluorescence, and this analysis indicated that Golgi morphology remained normal (Figure 1C). Furthermore, neither the alkaline earth metals Ca, Mg, and Sr nor the transition metals Cd, Cu, Co, Fe, and Zn induced loss of GPP130 (data not shown). Concentrations of Mn as low as 100 μM were sufficient to induce GPP130 degradation in both HeLa and AF-5 GABAergic cells (Supplemental Figure S1), whereas Mn-induced changes in cell cycle proteins and inflammatory mediators are not evident at concentrations <500 μM (Zhao *et al*., 2008; Milatovic *et al*., 2009). Loss of GPP130 in AF-5 cells is significant because it is the GABA-enriched neurons of the globus pallidus that are primarily affected in manganism (Sanchez *et al*., 2006; Crooks *et al*., 2007).

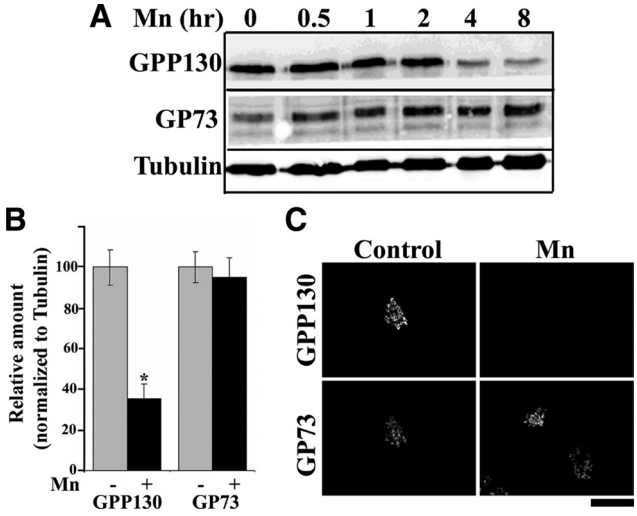

Figure 1. Mn induces the degradation of GPP130 in HeLa cells. (A) HeLa cells were treated with 500 μM $MnCl_2$ for the times indicated and subjected to immunoblot analyses to detect GPP130, GP73, and α-tubulin. (B) Levels of GPP130 and GP73 were quantified at the 0- and 8-h time points and normalized to tubulin levels (mean ± SE, $n = 3$; $p < 0.05$). (C) HeLa cells on coverslips were untreated or treated with 500 μM $MnCl_2$ for 8 h, fixed, and costained using anti-GPP130 (using the anti-GPP130 mAb) and anti-GP73 antibodies. Bar, 10 μm.

Mn-induced Degradation of GPP130 Occurs in the Lysosomal Compartment

The $t_{1/2}$ of Mn-induced degradation of GPP130 was much shorter than its ~18-h half-life (Linstedt *et al*., 1997), suggesting that Mn increases GPP130 degradation rather than decreasing its synthesis. Indeed, within 5 min of Mn addition, GPP130 began to redistribute from the Golgi to peripheral punctate structures and by 4 h all the remaining GPP130 was present in these structures (Figure 2A). To test whether the redistributed GPP130 was en route to lysosomes, we first expressed Rab7-GFP, a marker of MVBs, and exposed the cells to Mn for 2 h. Many GPP130 peripheral punctae were colabeled with Rab7-GFP (Figure 2B). At higher magnifications, Rab7-GFP was evident in a ring pattern lining the MVBs, with GPP130 either colocalized with the ring or present within the MVBs lumen lined by Rab7, strongly suggesting that GPP130 was undergoing internalization from the limiting membrane of MVBs (Figure 2C).

Additional evidence for the internalization of GPP130 into the lumen of MVBs was obtained by using a guanosine triphosphate (GTP)-restricted version of Rab5 (Rab5 Q79L), which produces giant MVBs by causing fusion of early endosomes (EEs) and MVBs (Stenmark *et al*., 1994). Indeed, GPP130 was clearly detectable within the lumen of the Rab5 Q79L-induced giant MVBs (Figure 2D, 4- and 8-h time points). In fact, small amounts of GPP130 could be detected within the lumen of these MVBs as early as 30 min after Mn (Figure 2D). The intralumenal localization of GPP130 within MVBs was confirmed by colabeling with EEA1, an EE-localized protein that lines the limiting membrane of the giant Rab5 Q79L-induced MVBs (Rosenfeld *et al*., 2001; Volpicelli *et al*., 2001; Rink *et al*., 2005). As expected, GPP130 was clearly detected inside the limiting membrane marked by both EEA1 and Rab5 Q79L (Supplemental Figure S2). Furthermore, 4 h after Mn, a large number of the cytoplasmic GPP130 punctae also colabeled with Lamp2, a lysosomal

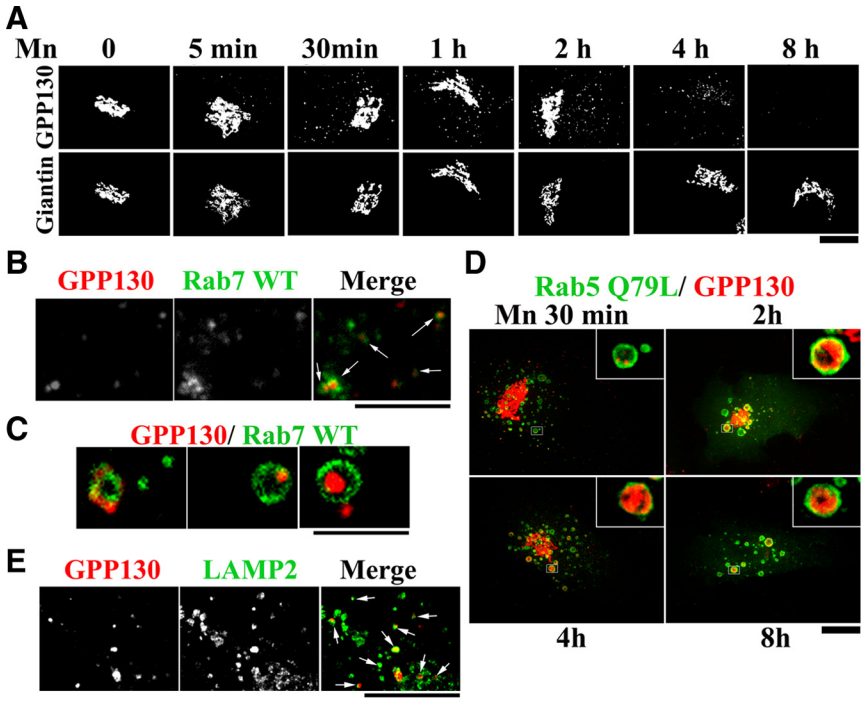

Figure 2. GPP130 redistributes to MVBs and lysosomes in response to Mn. (A) HeLa cells were treated with 500 μM $MnCl_2$ for the times indicated, fixed, and costained to detect GPP130 and giantin. Bar, 10 μm. (B and C) HeLa cells were transfected with GFP-tagged Rab7 WT, and 24 h after transfection they were treated with 500 μM $MnCl_2$ for 2 h and stained to detect GPP130. Arrowheads indicate overlap between GPP130 and Rab7-GFP. Bar, 4 μm (B) and 2 μm (C). (D) HeLa cells were transfected with Rab5 Q79L-GFP, exposed to 500 μM $MnCl_2$ for the times indicated, and subsequently stained to detect GPP130. Expression of Rab5 Q79L did not alter the basal localization of GPP130 (data not shown). Bar, 10 μm; insets, 5×. (E) HeLa cells were treated with 500 μM $MnCl_2$ for 4 h, fixed, and costained to detect GPP130 and Lamp2. Arrowheads indicate overlap between GPP130 and Lamp2. Bar, 4 μm.

marker (Figure 2E), indicating that GPP130 eventually trafficked to lysosomes.

To confirm that GPP130 was indeed degraded in lysosomes, we used pretreatment with the lysosomal protease inhibitors leupeptin and pepstatin (Nicoziani *et al.*, 2000). Although cultures treated with Mn alone showed substantial loss of GPP130, pretreatment with the inhibitors blocked the degradation of GPP130 after Mn, and these cells exhibited a dramatic accumulation of GPP130 in peripheral punctae (Figure 3A). Thus, under these conditions, GPP130 presumably trafficked to lysosomes but was not degraded due to the inhibitors. Note that cells pretreated with the inhibitors but no Mn exhibited a slightly increased level of GPP130 in peripheral puncta, indicating that the inhibitors were effective in blocking constitutive turnover of GPP130. Immunoblotting confirmed the ability of the lysosomal inhibitors to block the Mn-induced degradation of GPP130 (Figure 3B). Eight hours after Mn, GPP130 levels decreased to <35% of starting levels in control cultures. However, in cultures pretreated with the inhibitors, it remained ~80% of starting levels (Figure 3C). To rule out any contribution of proteasome-mediated degradation, cells were pretreated with the proteasome inhibitor lactacystin, and this did not block the Mn-induced degradation of GPP130 (data not shown). Thus, in response to Mn, GPP130 traffics out of the Golgi to MVBs and lysosomes where it is degraded.

Endocytosis and Early Endosome Trafficking Are Not Required for Mn-induced GPP130 Degradation

In general, proteins traffic from the Golgi to lysosomes using one of three well-characterized pathways: 1) Golgi to plasma membrane (PM), followed by endocytosis to EEs and trafficking via MVBs to lysosomes; 2) Golgi to EEs followed by trafficking to MVBs and lysosomes; or 3) Golgi directly to MVBs and then to lysosomes (Ihrke *et al.*, 2004; Scott *et al.*, 2004, Piper and Luzio, 2007). To test whether the Mn-in-

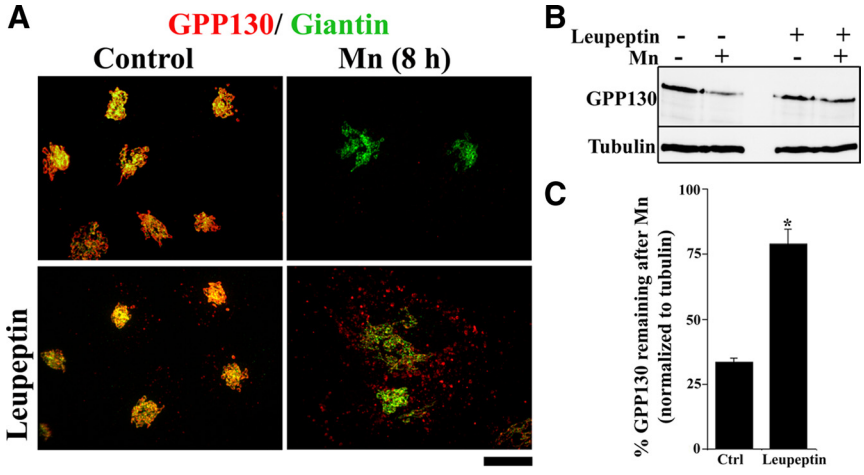

Figure 3. GPP130 is degraded in lysosomes after Mn. (A) HeLa cells were pretreated without or with leupeptin (100 μg/ml) and pepstatin (50 μg/ml) for 24 h (Nicoziani *et al.*, 2000), and then the media were adjusted to 0 or 500 μM $MnCl_2$ for 8 h. Coimmunostaining was used to detect GPP130 and giantin. Bar, 10 μm. (B) The experiment was also analyzed by immunoblot using antibodies against GPP130 and α-tubulin. (C) Quantitation of GPP130 levels normalized to tubulin levels with GPP130 levels in the absence of Mn as 100% (mean ± SE, n = 3; $p < 0.05$).

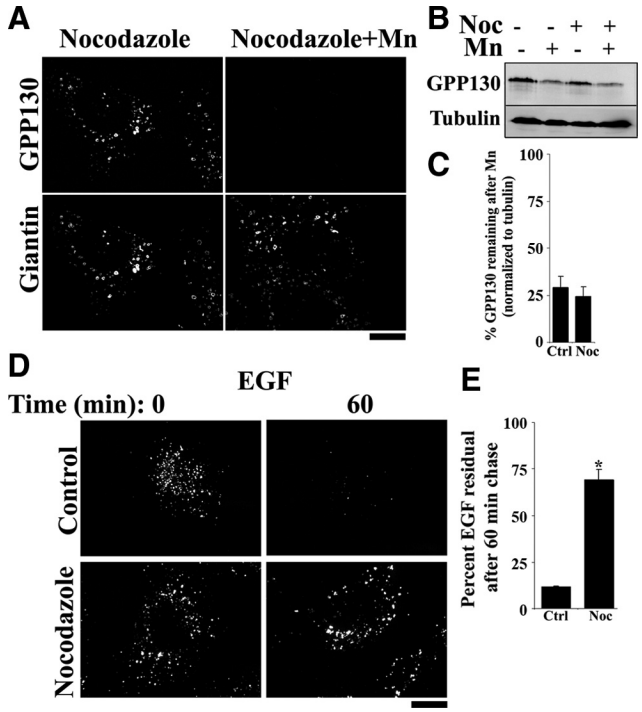

Figure 4. Depolymerizing microtubules with nocodazole does not block GPP130 degradation. (A) HeLa cells were pretreated for 3 h with or without nocodazole (1 μg/ml; Yadav *et al*., 2008), and then the media were adjusted to 0 or 500 μM $MnCl_2$ for 8 h. Coimmunostaining was with antibodies against GPP130 and giantin. Bar, 10 μm. (B and C) The experiment was also analyzed by immunoblot using antibodies against GPP130 and α-tubulin and quantified with GPP130 levels normalized to tubulin and in the absence of Mn expressed as 100% (mean ± SE, n = 3; $p > 0.05$). (D) HeLa cells were treated with nocodazole, and then the EGF degradation assay was performed. Bar, 10 μm. (E) Quantitation of the mean EGF fluorescence per cell with levels at time 0 expressed as 100% (mean ± SE, n > 12 cells/condition/time point; $p < 0.05$).

duced trafficking of GPP130 to MVBs required its transit through the PM, we used a dominant-negative version of the GTPase dynamin II (Dyn II K44A), which is an effective inhibitor of most types of endocytosis (Conner and Schmid, 2003). Significantly, dominant-negative dynamin II did not have any discernible effect on the loss of GPP130 in response to 8 h of Mn exposure; yet, as expected, it was effective in inhibiting internalization of fluorescent EGF (Supplemental Figure S3).

Because endocytosis was not required, we next used a dominant-negative Rab5 construct (Rab5 S34N), which inhibits trafficking to/from EEs (Stenmark *et al*., 1994), to test whether GPP130 might traffic through EEs en route to degradation. However, trafficking to EEs did not seem necessary because Rab5 S34N failed to block Mn-induced GPP130 degradation, whereas as a control, it did block degradation of internalized fluorescent EGF (Supplemental Figure S4).

To further test the role of EEs, we disrupted the microtubule network by using nocodazole. Maturation of EEs into MVBs requires a functional microtubule network (Gruenberg *et al*., 1989). Golgi positioning is also dependent on microtubules, but the isolated Golgi ministacks present in nocodazole-treated cells remain transport competent (Hirschberg *et al*., 1998; Thyberg and Moskalewski, 1999, Yadav *et al*., 2008). Indeed, even though the Golgi was fragmented, loss of GPP130 in response to Mn seemed normal in nocodazole-treated cells (Figure 4A). Unlike the transient transfections described above, nocodazole treatment affects all cells in the population, thus allowing confirmation by immunoblotting. GPP130 degradation was clearly evident by immunoblot analysis, and there was no statistical difference between residual GPP130 levels in control and nocodazole-treated cells (Figure 4, B and C). In contrast, EGF degradation was significantly impaired under these conditions (Figure 4D), with ~70% of the endocytosed EGF resisting degradation after nocodazole, compared with ~10% in controls (Figure 4E). Thus, the studies in this section indicate that Mn-induced GPP130 redistribution to lysosomes is independent of both endocytosis and EE trafficking, suggesting that GPP130 takes a direct path from the Golgi to MVBs en route to degradation.

Mn-induced Degradation of GPP130 Is Rab7 Dependent

The small GTPase Rab7 is required for trafficking from MVBs to lysosomes and for the formation of functionally mature lysosomes (Bucci *et al*., 2000, Vanlandingham and Ceresa, 2009). Dominant-negative Rab7 (Rab7 T22N) inhibits MVB-to-lysosome trafficking (Bucci *et al*., 2000; Vanlandingham and Ceresa, 2009), causing MVBs to enlarge (Vanlandingham and Ceresa, 2009), but it does not affect endocytosis or trafficking through EEs (Papini *et al*., 1997; Vitelli *et al*., 1997, Bucci *et al*., 2000, Vanlandingham and Ceresa, 2009). Indeed, in accordance with previous work (Papini *et al*., 1997), EGF was efficiently degraded in cells expressing Rab7 WT, but its degradation was blocked by expression of Rab7 T22N (Supplemental Figure S5). To test the role of Rab7 in Mn-induced GPP130 degradation, we examined cells expressing Rab7 WT and T22N, neither of which altered the basal localization of GPP130 in the Golgi. GPP130 degradation was unaffected by Rab7 WT, but in cells expressing Rab7 T22N, GPP130 dramatically accumulated in large peripheral puncta after Mn (Figure 5A). In cells expressing Rab7 WT, the levels of GPP130 decreased to <25% of starting levels after 8 h of Mn. In cells expressing Rab7 T22N the

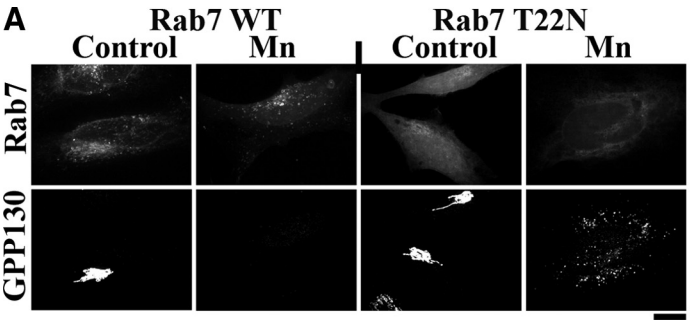

Figure 5. Mn-induced degradation of GPP130 is Rab7 dependent. (A) HeLa cells were transfected with GFP-tagged Rab7 WT or Rab7 T22N, and 24 h after transfection they were treated with 500 μM $MnCl_2$ for 8 h or left untreated. Cells were then fixed, stained, and imaged to detect GPP130 and GFP. Bar, 10 μm. (B) Quantitation of the mean GPP130 fluorescence per cell with levels in the absence of Mn normalized to 100% (mean ± SE, n > 12 cells/construct/time point; $p < 0.05$).

levels of GPP130 remained at ~70% of the starting Golgi signal (Figure 5B). Thus, in the presence of dominant-negative Rab7, Mn-induced the trafficking of GPP130 out of the Golgi but its degradation was blocked. The accumulation of GPP130 in large cytoplasmic puncta in Mn-treated cells expressing Rab7 T22N is consistent with it being trapped in an enlarged MVB compartment.

Overall, extracellular Mn induces the redistribution of GPP130 from the Golgi to the interior of MVBs en route to degradation in lysosomes. The dependence of the trafficking on Rab7 in combination with its independence from dynamin, Rab5, and microtubules indicates that the trafficking is direct from the Golgi to MVBs.

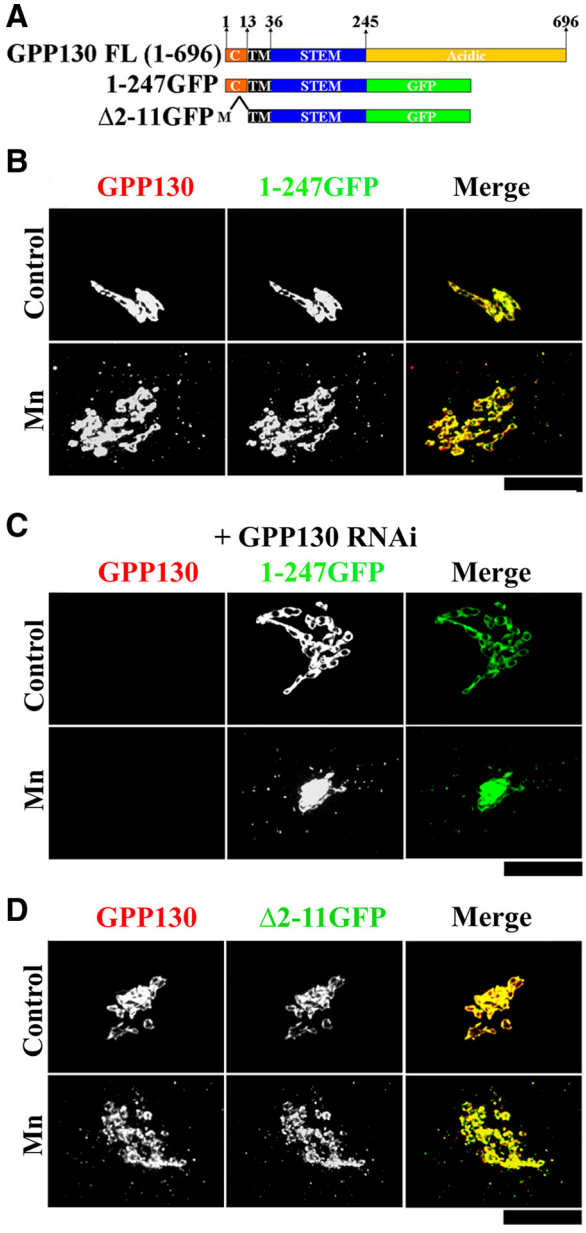

Figure 6. The GPP130 acidic and cytoplasmic domains are dispensable. (A) Schematic of full-length GPP130 and the deletion constructs lacking the lumenal acidic domain with and without the cytoplasmic domains. Position and residue numbers of cytoplasmic (C), transmembrane (TM), stem, and acidic domains are indicated. "M" indicates the first methionine. (B) HeLa cells were transfected with $GPP130_{1-247}$-GFP. Twenty-four hours after transfection, they were exposed to 100 μg/ml cycloheximide for 2 h and then adjusted to 0 or 500 μM $MnCl_2$ for 2 h. Cells were then fixed, stained, and imaged to detect GPP130 and GFP. Bar, 10 μm. (C) HeLa cells were siRNA-transfected to knockdown endogenous GPP130. After 2 d, the cells were retransfected with an RNAi-immune version of $GPP130_{1-247}$-GFP, and after 24 h they were treated with cycloheximide and Mn as described above. The cells were then fixed, stained, and imaged to detect endogenous GPP130 (using anti-GPP130 mAb against acidic domain) and GFP. Bar, 10 μm. (D) HeLa cells were transfected with $GPP130_{\Delta 2\text{-}11}$-GFP, treated with cycloheximide and Mn as described above, and processed to detect GPP130 and GFP. Bar, 10 μm.

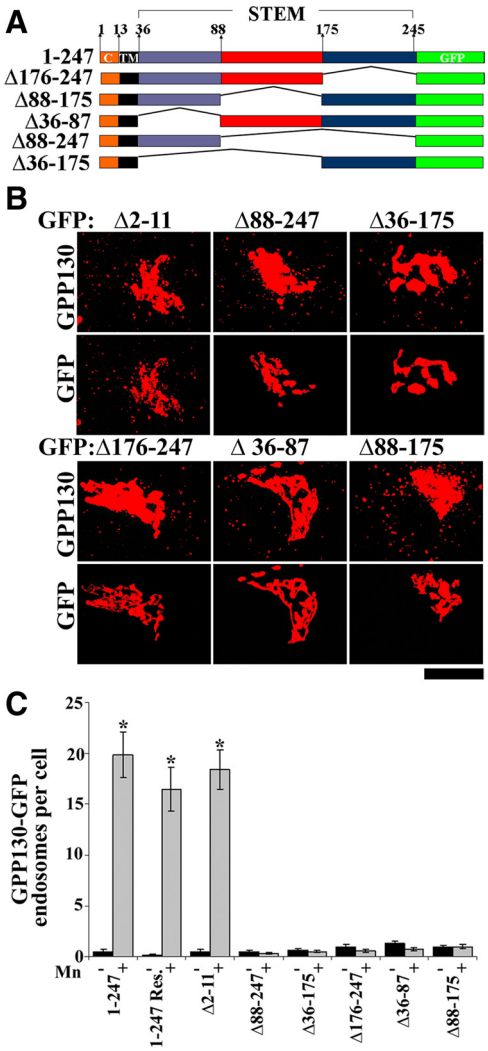

Figure 7. Deletions in the stem domain of GPP130 abolish its sensitivity to Mn. (A) Schematic of the deletion constructs used in this figure. All deletions were made on $GPP130_{1-247}$-GFP. (B) Cells were transfected with the indicated constructs, and after 24 h they were exposed to cycloheximide for 2 h then adjusted to 500 μM Mn for 2 h. After processing, GPP130 and GFP were imaged in the same cells. Thresholding was used to enhance visualization of endosome with identical thresholds applied to all constructs in a given channel. Bar, 10 μm. (C) Quantitation of the number of GFP endosomes per cell with (gray) and without (black) Mn for each GPP130 construct. $GPP130_{1-247}$-GFP was also analyzed after rescue (Res.). The Mn-induced increase in GFP endosomes per cell was statistically significant for $GPP130_{1-247}$-GFP, $GPP130_{1-247}$-GFP rescue, and $GPP130_{\Delta 2\text{-}11}$-GFP (mean ± SE, $n > 25$ cells for each construct with and without Mn; $p < 0.05$) but not the other stem deleted constructs ($p > 0.05$).

The Acidic Domain of GPP130 Is Not Required for Mn-sensitive Trafficking

GPP130 is a single-pass transmembrane protein with a short cytoplasmic domain and a two-part lumenal domain in which the first 210 residues form a coiled-coil stem domain and the final 451 residues form a domain highly enriched in acidic amino acids. One possibility was that the acidic residues interacted with Mn and somehow altered the function of the coiled-coil stem domain, which contains the sequence features that are necessary and sufficient for GPP130 Golgi localization (Bachert *et al.*, 2001). To test the role of the acidic domain, we deleted it by replacing it with GFP (Figure 6A). The resulting construct, $GPP130_{1\text{-}247}$-GFP, was localized to the Golgi, and upon exposure to Mn for 2 h, redistributed to endosomal structures that colabeled with endogenous GPP130 (Figure 6B; see Figure 7C for quantification). Thus, the acidic domain seemed dispensable. To rule out the possibility that $GPP130_{1\text{-}247}$-GFP was simply associating with endogenous GPP130, we carried out rescue after RNA interference (RNAi) (Puthenveedu and Linstedt, 2004, Natarajan and Linstedt, 2004). Cells expressing $GPP130_{1\text{-}247}$-GFP, but undetectable endogenous GPP130, were readily identified using GFP fluorescence to detect $GPP130_{1\text{-}247}$-GFP and an antibody against the acidic domain to specifically detect endogenous GPP130 (see *Materials and Methods*; Linstedt *et al.*, 1997). In these cells $GPP130_{1\text{-}247}$-GFP was Golgi localized and redistributed to endosomes upon Mn addition (Figure 6C; see Figure 7C for quantification).

Mn-induced GPP130 Trafficking and Internalization into MVBs Occurs without the GPP130 Cytoplasmic Domain

Because the acidic domain was not required, we next focused attention on the cytoplasmic domain. Both AP3 and GGA adaptors mediate sorting of proteins from the Golgi directly to MVBs, and each depends on cytoplasmic domain sorting signals. The AP3-binding sequence motif YXXΦ (Ihrke *et al.*, 2004) is not present in the 12-residue GPP130 cytoplasmic domain, but this domain does contain two lysines that, in principle, could be ubiquinated, creating a GGA binding site (Scott *et al.*, 2004; Piper and Luzio, 2007; Risinger and Kaiser, 2008). To test the role of the cytoplasmic domain, it was deleted from $GPP130_{1\text{-}247}$-GFP to create $GPP130_{\Delta 2\text{-}11}$-GFP (Figure 6A). Remarkably, $GPP130_{\Delta 2\text{-}11}$-GFP was targeted to the Golgi and redistributed to endosomes upon Mn addition (Figure 6D), as did a GPP130 construct in which the two cytoplasmic lysines were substituted to alanines (data not shown). We also confirmed that $GPP130_{\Delta 2\text{-}11}$-GFP was responsive to Mn in the absence of endogenous GPP130 (data not shown).

Furthermore, when cotransfected with Rab5 Q79LΔGFP, $GPP130_{\Delta 2\text{-}11}$-GFP was present within the lumen of the Rab5-induced giant MVBs (detected using EEA1) after Mn (Supplemental Figure S6), indicating that even internalization into MVBs was independent of the GPP130 cytoplasmic domain. Thus, the cytoplasmic domain of GPP130, and by extension any possible posttranslational modification of this domain such as ubiquitination, was not required for the Mn-induced trafficking of GPP130 to MVBs. In sum, neither the acidic nor the cytoplasmic domains mediate Mn-induced down-regulation of GPP130, suggesting a role for the transmembrane or stem domains.

Stem Domain Deletions Alter Intra-Golgi Localization and Block Mn Sensitivity

The coiled-coil stem domain of GPP130 mediates its Golgi targeting (Bachert *et al.*, 2001). Given that our investigation of the *cis*-acting elements underlying the Mn response required a Golgi-targeted construct before Mn treatment, we were fortu-

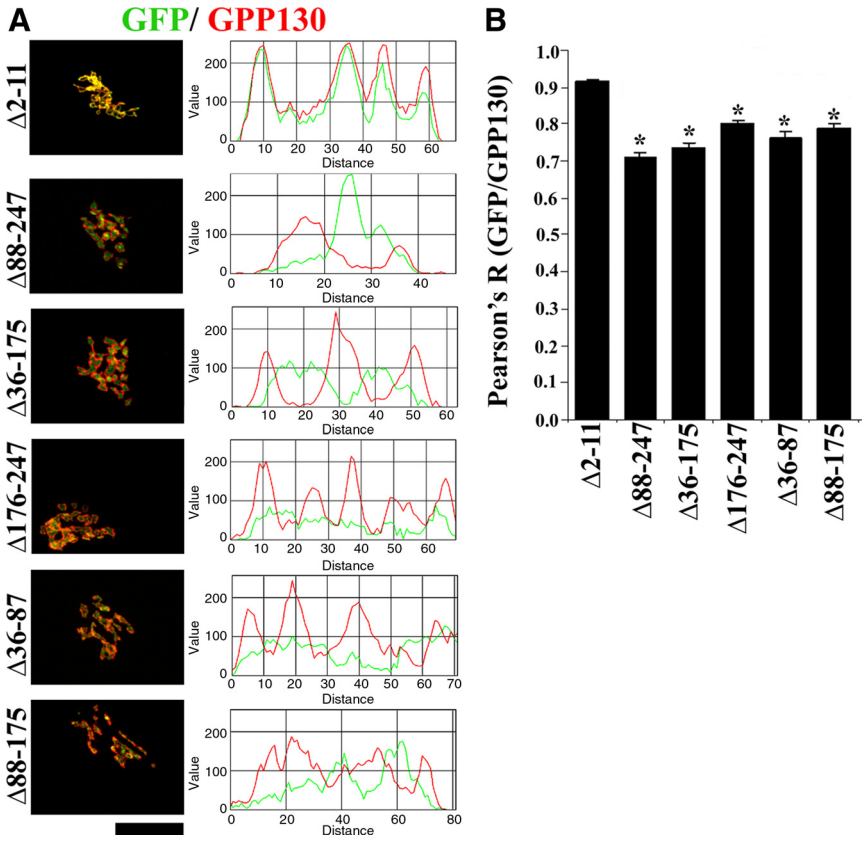

Figure 8. Deletions in the stem domain change the intra-Golgi localization of GPP130. (A) HeLa cells were transfected with the indicated constructs, exposed to cycloheximide for 4 h, and processed to detect endogenous GPP130 (using the anti-acidic domain mAb) and GFP. Line plots to assess overlap between endogenous GPP130 (red) and GFP (green) signals accompany individual immunofluorescence panels. Bar, 10 μm. (B) Plot of the Pearson's coefficient for colocalization between GFP and endogenous GPP130 signals for the indicated constructs. Pearson's coefficient for $GPP130_{\Delta 2\text{-}11}$-GFP was significantly greater than all the other constructs (mean ± SE, n > 10 cells/construct; $p < 0.05$).

nate that the stem domain was subdivided previously and found to contain independently acting Golgi localization determinants within residues 36-87 and 176-245 (Bachert *et al*., 2001). Intriguingly, the intervening sequence 88–175 confers localization to endosomes when isolated from the Golgi signals (Bachert *et al*., 2001). To test the role of these subdomains, each was deleted, singly or in combination, from $GPP130_{1-247}$-GFP (Figure 7A). The resulting constructs each contained at least one Golgi determinant and were Golgi-localized (Supplemental Figure S7). Nevertheless, none of these constructs responded to Mn additions, whereas, as a positive control, the $GPP130_{\Delta 2-11}$-GFP again did (Figure 7B). The lack of a Mn response in the stem-deleted constructs was not a failure of the cells to respond to Mn because, in the same cells, endogenous GPP130 redistributed to endosomes (Figure 7B). Quantification clearly supported the conclusion that each of these deletions from the stem domain blocked Mn-induced redistribution (Figure 7C). These assays took advantage of the presence of endogenous GPP130 to confirm an intact cellular Mn response, which necessitated treatment with cycloheximide to limit overexpression and mistargeting of the transfected proteins. To avoid the cytotoxic effects of cycloheximide, the assays were carried out at the 2-h time point, leaving open the possibility that the mutations merely delayed rather than blocked the Mn response. To carryout the analysis at a later time point and avoid the cytotoxic effects of prolonged cycloheximide treatment, we repeated the experiment with two siRNA-immune constructs after GPP130 knockdown that limited the total amount of GPP130 present and allowed for proper targeting of the transfected constructs in the absence of cycloheximide. Even after 8 h of Mn treatment, the Mn-insensitive construct $GPP130_{\Delta 88-247}$-GFP remained stably localized to the Golgi, whereas the control construct $GPP130_{1-247}$-GFP redistributed and was degraded leaving only residual levels (Supplemental Figure S8). Thus, deletion in the GPP130 stem domain caused a profound block in its Mn responsiveness.

A possible explanation for the puzzling result that all stem domain deletions blocked Mn sensitivity emerged when the targeting of the constructs was more precisely determined. Taking advantage of the specific recognition of endogenous GPP130 by the antibody against the acidic domain, we carried out colocalization analysis of endogenous GPP130 with the stem-deleted constructs in cells before the addition of Mn. Whereas the GPP130 responsive construct $GPP130_{\Delta 2-11}$-

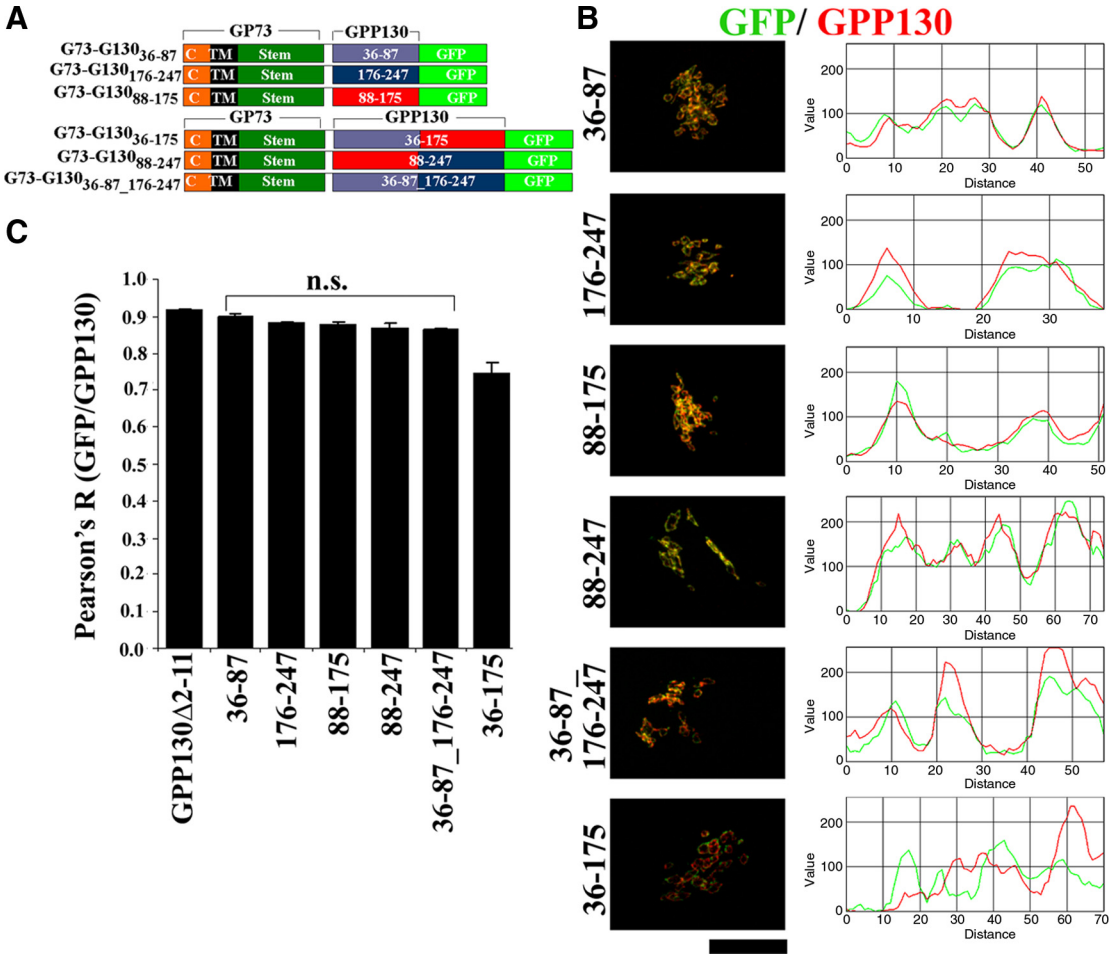

Figure 9. Chimeric GP73-GPP130 constructs are targeted to the *cis*-Golgi. (A) Schematic of the chimeric constructs. (B) HeLa cells were transfected with chimeric GP73-GPP130 constructs and treated with cycloheximide for 4 h and processed to detect endogenous GPP130 (using anti-acidic domain mAb) and GFP. Line plots for the overlap between endogenous GPP130 (red) and GFP (green) channels are shown. Bar, 10 μm. (C) Plot of the Pearson's coefficient for colocalization between GFP and endogenous GPP130 signals for the indicated constructs. The Pearson's coefficient for the $GPP130_{\Delta 2-11}$-GFP construct is also included for comparison. Except $G73\text{-}G130_{36-175}$-GFP, there was no significant difference between the Pearson's coefficients for $GPP130_{\Delta 2-11}$-GFP and the chimeric constructs (mean ± SE, $n > 10$ cells/construct; $p > 0.05$).

GFP colocalized with endogenous GPP130, the stem-deleted constructs did not (Figure 8A). For each of these constructs, the GFP signal was adjacent to the endogenous GPP130 staining. The difference was particularly striking when the endogenous staining took on ring-like patterns. The GFP signal was clearly inside these rings. Line plots of the fluorescent intensity also showed the lack of colocalization (Figure 8A). Furthermore, quantitative analysis using the Pearson's coefficient confirmed that there was a statistically significant decrease in the colocalization of the stem-deleted constructs with endogenous GPP130 compared with that of $GPP130_{\Delta 2\text{-}11}$-GFP (Figure 8B). It is typical for the staining of *cis*- or *medial*-Golgi markers to ring that of *trans*-Golgi or TGN markers under these fixation conditions (Puri *et al.*, 2002), suggesting that the deletions in the stem domain of GPP130 had caused the proteins to shift their localization toward the TGN. Indeed, both the stem-deleted constructs and the TGN marker golgin97 (Yoshino *et al.*, 2003) were found inside the same Golgi ring structures (data not shown). Thus, deletions in the stem domain unexpectedly displaced the protein from the *cis*-Golgi, perhaps by weakening interactions required for GPP130 retrieval, and this correlated with a loss of sensitivity to Mn.

GPP130 Stem Domain Confers Mn Sensitivity to a Related cis-Golgi Protein

Based on the idea that *cis*-Golgi targeting in conjunction with one or more of the GPP130 stem subdomains might be needed for the Mn response, we took advantage of the fact that GP73 is localized to the *cis*-Golgi and shares features with GPP130, including a coiled-coil stem domain that targets GP73 to the *cis*-Golgi (Puri *et al.*, 2002). Thus, a set of constructs was generated in which the stem subdomains of GPP130 were placed, singly or in combinations, after the stem domain of GP73 and before a C-terminal GFP (Figure 9A). Colocalization analysis identical to that described above was carried out on these constructs and indicated that the constructs, with one exception, were indeed localized to the *cis*-Golgi. The GFP fluorescence was strikingly similar to endogenous GPP130 staining, and the two yielded correlated line plots (Figure 9B). Furthermore, quantitative analyses using Pearson's coefficients confirmed that, with one exception, there was no statistical difference between the colocalization of the chimeric constructs and endogenous GPP130 compared with that of $GPP130_{\Delta 2\text{-}11}$-GFP (Figure 9C). Even the one construct that yielded noncolocalization (G73-$G130_{36\text{-}175}$-GFP) was still likely to have been targeted to the *cis*-Golgi. The fluorescence of this construct defined rings surrounding endogenous GPP130, suggesting that endogenous GPP130 may have been pushed out of the *cis*-Golgi by this construct. Competitive interactions in Golgi targeting of GPP130 and GP73 have been observed previously (Puri *et al.*, 2002). Regardless, most, if not all, the chimeric constructs were in the *cis*-Golgi, allowing a test of whether *cis*-Golgi localization of the stem subdomains was sufficient to confer Mn sensitivity.

To test for Mn sensitivity, cells expressing each construct were exposed to Mn for 2 h, and redistribution of the construct as well as endogenous GPP130 in the same cells was determined. Remarkably, constructs with any two of the three subdomains yielded clear redistribution, whereas constructs with individual subdomains did not (Figure 10, A and B). Endogenous GPP130 responded even in cells where a construct did not thus confirming that the cellular Mn response was intact. Although the N-terminal segment of the stem domain, residues 36-87, failed to respond in isolation, it seemed to contribute the most. Of the three constructs with combinations of the subdomains, those with the N-terminal subdomain (G73-$G130_{36\text{-}175}$-GFP and G73-$G130_{36\text{-}87\_176\text{-}247}$-GFP) yielded a 100% response rate, and the level of response, as judged by the number of peripheral punctae per cell, was high (Figure 10B). In contrast, for the construct lacking this subdomain (G73-$G130_{88\text{-}247}$-GFP), the response rate was only 65% and the number of puncta per cell was significantly lower (Figure 10B).

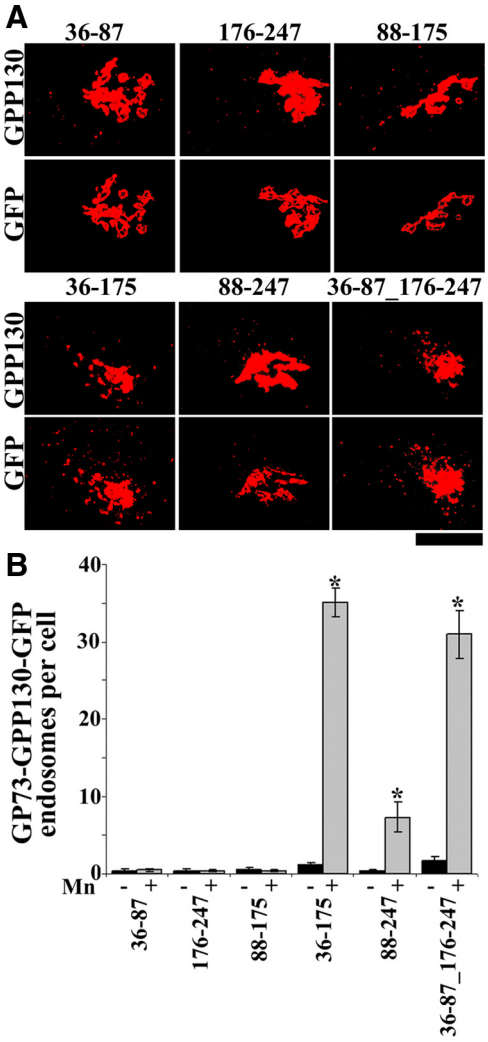

Figure 10. Chimeric GP73-GPP130 constructs respond to Mn. (A) HeLa cells were transfected with GP73-GPP130 chimeric constructs, and after 24 h they were treated with cycloheximide for 2 h and adjusted to 500 μM Mn for 2 h. The cells were processed to detect GPP130 and GFP. Images depicted are uniformly thresholded to maximize visualization of endosomes. Bar, 10 μm. (B) Quantitation of the number of GFP endosomes per cell with (gray) and without (black) Mn for the indicated GP73-GPP130 chimeric constructs. The Mn-induced increase in GFP endosomes per cell was statistically significant for G73-$G130_{36\text{-}175}$-GFP, G73-$G130_{88\text{-}247}$-GFP, and G73-$G130_{36\text{-}87\_176\text{-}247}$-GFP (mean $\pm$ SE, $n > 25$ cells for each construct with and without Mn; $p < 0.05$) but not the other chimeric constructs ($p > 0.05$).

In sum, the stem domain of GPP130 represents a transferable determinant for Mn-sensitive targeting to MVBs from the *cis*-Golgi.

DISCUSSION

Our study identifies the *cis*-Golgi glycoprotein GPP130 as a Mn-responsive protein. Extracellular Mn triggered exit of

GPP130 from the Golgi and trafficking directly to MVBs where it was internalized to intralumenal vesicles and ultimately degraded by lysosomal hydrolases. The Mn-induced trafficking of GPP130 was initiated within minutes and required its lumenal stem domain. Proper targeting of this stem domain to the *cis*-Golgi seemed to be important in conferring Mn sensitivity to GPP130. The stem domain was also sufficient in that appending it to another *cis*-localized Golgi protein caused the resulting chimera to traffic out of the Golgi in response to Mn. These findings show that Mn alters the intracellular trafficking of a mammalian protein and identify, within the protein, a novel transferable Mn response element.

Although we considered the possibility that GPP130 redistribution in response to Mn was caused by a block in bypass pathway trafficking, this is unlikely. As stated, GPP130 cycles out of the Golgi and is retrieved from EEs via the bypass pathway (Linstedt *et al*., 1997; Bachert *et al*., 2001; Puri *et al*., 2002; Natarajan and Linstedt, 2004). If Mn were to induce a block in the bypass pathway retrieval of GPP130, GPP130 might be diverted from EEs to MVBs and over time, undergo degradation. However, three lines of evidence argue that targeting of GPP130 to MVBs after Mn was not secondary to a block in bypass pathway retrieval. First, trafficking from EEs to MVBs, the pathway for diversion out of the bypass pathway, was not required for Mn-induced trafficking of GPP130 to MVBs. Second, GPP130 residues 88-175, which are required for cycling in the bypass pathway, were not required for Mn sensitivity. Third, Mn did not change the localization of other proteins trafficking in the bypass pathway such as GP73. Because Golgi localization of bypass pathway proteins is pH sensitive, the last point also implies that Mn did not alter intralumenal pH. Furthermore, the unperturbed Golgi localization of GP73 argues that levels of GPP130 remaining after Mn were sufficient to support bypass pathway function (Natarajan and Linstedt, 2004). Thus, Mn did not inhibit the bypass pathway but rather induced a change in the sorting of GPP130 directing it from the Golgi to MVBs.

The Mn responsiveness of GPP130 was mapped to its lumenal stem domain. This domain, when localized to the *cis*-Golgi, represented a transferable Mn-sensitive signal for trafficking from the Golgi to MVBs. Our results raise three provocative questions. First, how could the stem domain of GPP130 mediate Mn-sensitive trafficking? Second, what could be the possible physiological relevance of the Mn-induced degradation of GPP130? And third, why does the stem domain of GPP130 have to be targeted to the *cis*-Golgi to be responsive to Mn?

We suggest the possibility that, in the presence of Mn, the GPP130 stem domain binds one or more proteins in the *cis*-Golgi. The GPP130 binding partner could be a *cis*-Golgi resident or newly synthesized cargo transiting through the Golgi. Formation of the hypothetical complex might block Golgi localization signals while exposing lysosomal targeting signals, thereby targeting the entire complex to lysosomes for degradation. Because the cytoplasmic domain of GPP130 is dispensable, it is likely that the binding partner contributes cytoplasmically disposed signals for interactions with specific adaptors leading to trafficking to, and internalization in, MVBs.

Given the physiological context, it is conceivable that the putative GPP130 binding partner is a Mn transporter undergoing homeostatic regulation. GPP130 could potentially bind a newly synthesized pool of a Mn transporter transiting through the Golgi en route to the plasma membrane and target it for degradation. This would be analogous to yeast cells diverting newly synthesized Mn transporter to the vacuole to inhibit further uptake of Mn at the plasma membrane (Jensen *et al*., 2009). GPP130 could also potentially regulate the trafficking of the newly synthesized pool of SPCA1, the *trans*-Golgi–localized Mn and Ca transporter (Behne *et al*., 2003), in a Mn-dependent manner. Thus, GPP130 might conceivably interact with any Mn-related activity, known or unknown, entering the *cis*-Golgi and, in the presence of excess Mn, divert it to lysosomes as a means of down-regulation.

In this scenario, GPP130 would act as a targeting cofactor conferring part of the cellular Mn response. This would be similar to the situation for the yeast high-affinity iron permease Ftr1, which associates with its cofactor Fet3 (Stearman *et al*., 1996). Fet3 is an oxidase that uses Cu^{2+} to convert Fe^{3+} to Fe^{2+} so that Ftr1 can internalize Fe^{2+}. In the absence of Cu^{2+}, the complex is trapped intracellularly, but when Fet3 binds Cu^{2+} the complex of Fet3/Ftr1 traffics to the plasma membrane (Gaxiola *et al*., 1998).

Deletions of part of the GPP130 stem domain caused an apparent shift in localization from *cis*-cisternae to a more *trans*-position and also a loss of Mn sensitivity, which could be restored by the *cis*-targeting information in GP73. A variety of observations suggest that the steady-state localization of GPP130 in the *cis*-Golgi depends largely on retrieval within the Golgi and from endosomes (Linstedt *et al*., 1997; Puri *et al*., 2002; Bachert *et al*., 2001). Thus, it is likely that deletions in the stem domain, which contain GPP130-targeting determinants (Bachert *et al*., 2001), reduce the efficiency of its retrieval causing a shift in its localization to a more *trans*-compartment. Although it is unclear why the Mn response was restricted to *cis*-cisternae, if the GPP130 binding partner proposed to bind GPP130 in elevated Mn were *cis*-localized, trans-localized GPP130 constructs would fail to form the complex needed for the altered trafficking.

Overall, our studies identify a Mn-responsive protein in mammalian cells, describe its trafficking route, and begin to elucidate sequence requirements within the molecule for the response. This discovery may lead to a better understanding of intracellular Mn homeostasis and the pathobiology of Mn-induced neurodegeneration in humans.

ACKNOWLEDGMENTS

We thank Ritika Tewari for performing the Annexin-V-FITC staining and Tina Lee and Manojkumar Puthenveedu for comments on the manuscript. Funding was provided by the National Institutes of Health grant R01 GM-084111 (to A.D.L.).

REFERENCES

Aschner, M., Vrana, K. E., and Zheng, W. (1999). Manganese uptake and distribution in the central nervous system (CNS). Neurotoxicology *20*, 173–180.

Au, C., Benedetto, A., and Aschner, M. (2008). Manganese in eukaryotes. Neurotoxicology *29*, 569–576.

Bachert, C., Lee, T. H., and Linstedt, A. D. (2001). Lumenal endosomal and Golgi-retrieval determinants involved in pH-sensitive targeting of an early Golgi protein. Mol. Biol. Cell *12*, 3152–3160.

Behne, M. J., Tu, C. L., Aronchik, I., Epstein, E., Bench, G., Bikle, D. D., Pozzan T., and Mauro, T. M. (2003). Human keratinocyte ATP2C1 localizes to the Golgi and controls Golgi Ca^{2+} stores. J. Invest. Dermatol. *121*, 688–694.

Bouchard, M., Laforest, F., Vandelac, L., Bellinger, D., and Mergler, D. (2007). Hair manganese and hyperactive behaviours: pilot study of school-age children exposed through tap water. Environ. Health Perspect. *115*, 122–127.

Bucci, C., Thomsen, P., Nicoziani, P., McCarthy, J., and van Deurs, B.(2000). Rab 7: a key to lysosome biogenesis. Mol. Biol. Cell *11*, 467–480.

Conner, S. D., and Schmid, S. L. (2003). Regulated portals of entry into the cell. Nature *422*, 37–44.

Crooks, D., Welch, N., and Smith, D. R. (2007). Low-level manganese exposure alters glutamate metabolism in GABAergic AF5 cells. Neurotoxicology *28*, 548–554.

Culotta, V. C., Yang, M., and Hall, M. D. (2005). Manganese transport and trafficking: lessons learned from *Saccharomyces cerevisiae*. Eukaryot. Cell *4*, 1159–1165.

Damke, H., Baba, T., Warnock, D. E., and Schmid, S. L. (1994). Induction of mutant dynamin specifically blocks endocytic coated vesicle formation. J. Cell Biol. *127*, 915–934.

Deng, Y., Guo, Y., Watsom, H., Au, W. C., Shakoury-Elizeh, M., Basrai, M. A., Bonifacino, J. S., and Philpott, C. C. (2009). Gga2 mediates sequential ubiquitin-independent and ubiquitin-dependent steps in the trafficking of ARN1 from the trans-Golgi network to the vacuole. J. Biol. Chem. *284*, 23830–23841.

Denizot, F., and Lang, R. (1986). Rapid colorimetric assay for cell growth and survival. Modifications to the tetrazolium dye procedure giving improved sensitivity and reliability. J. Immunol. Methods *22*, 271–277.

Gaxiola, R. A., Yuan, D. S., Klausner, R. D., and Fink, G. R. (1989). The yeast CLC channel functions in cation homeostasis. Proc. Natl. Acad. Sci. USA *95*, 4046–4050.

Gitler, A. D., *et al*. (2009). alpha-Synuclein is part of a diverse and highly conserved interaction network that includes PARK9 and manganese toxicity. Nat. Genet. *41*, 308–315.

Gruenberg, J., Griffiths, G., and Howell, K. E. (1989). Characterization of the early endosome and putative endocytic carrier vesicles in vivo and with an assay of vesicle fusion in vitro. J. Cell Biol. *108*, 1301–1316.

Hirschberg, K., Miller, C. M., Ellenberg, J., Presley, J. F., Siggia, E. D., Phair, R., and Lippincott-Schwartz, J. (1998). Kinetic analysis of secretory protein traffic and characterization of Golgi to plasma membrane transport intermediate in living cells. J. Cell Biol. *143*, 1485–1503.

Ihrke, G., Kyttala, A., Russell, M.R.G., Rous, B. A., and Luzio, J. P. (2004). Differential use of two AP-3-mediated pathways by lysosomal membrane proteins. Traffic *5*, 946–962.

Jensen, L. T., Carroll, M. C., Hall, M. D., Harvey, C. J., Beese, S. E., Culotta, V. C. (2009). Down-regulation of a manganese transporter in the face of metal toxicity. Mol. Biol. Cell *20*, 2810–2819.

Kauppi, M., Simonsen, A., Bremnes, B., Vieira, A., Callaghan, J., Stenmark, H., and Olkkonen, V. M. (2002). The small GTPase Rab22 interacts with EEA1 and controls endosomal membrane trafficking. J. Cell Sci. *115*, 899–911.

Kitzberger, R., Madl, C., and Ferenci, P. (2005). Wilson disease. Metab. Brain Dis. *20*, 295–302.

La Fontaine, S., and Mercer, J. (2007). Trafficking of the copper-ATPases, ATP7A and ATP7B: role in copper homeostasis. Arch. Biochem. Biophys. *463*, 149–167.

Linstedt, A. D., Mehta, A., Suhan, J., Reggio, H., and Hauri, H. P. (1997). Sequence and overexpression of GPP130/GIMPc: evidence for saturable pH-sensitive targeting of a type II early Golgi membrane protein. Mol. Biol. Cell *8*, 1073–1087.

Milatovic, D., Zaja-Milatovic, S., Gupta, R. C., Yu, Y., and Aschner, M. (2009). Oxidative damage and neurodegeneration in manganese-induced neurotoxicity. Toxicol. Appl. Pharmacol. *240*, 219–225.

Missiaen, L., Raeymaekers, L., Dode, L., Vanoevelen, J., Baelen, K. V., Parys, J. B., Callewaert, G., Smedt, H. D., Segaert, S., and Wuytack, F. (2004). SPCA1 pumps and Hailey-Hailey disease. Biochem. Biophys. Res. Commun. *322*, 1204–1213.

Natarajan, R., and Linstedt, A. D. (2004). A cycling cis Golgi protein mediates endosome-to-Golgi trafficking. Mol. Biol. Cell *15*, 4798–4806.

Nicoziani, P., Vilhardt, F., Llorente, A., Hilout, L., Courtoy, P. J., Sandvig, K., and van Deurs, B. (2000). Role of dynamin in late endosome dynamics and trafficking of cation-independent mannose-6-phosphate receptor. Mol. Biol. Cell *11*, 481–495.

Olanow, C. W. (2004). Manganese-induced Parkinsonism and Parkinson's disease. Ann. NY Acad. Sci. *1012*, 209–223.

Papini, E., Satin, B., Bucci, C., de Bernard, M., Telford, J. L., Manetti, R., Rappouli, R., Zerial, M., and Montecucco, C. (1997). The small GTPase rab7 is essential for cellular vacuolation induced by *Helicobacter pylori* cytotoxin. EMBO J. *16*, 15–24.

Piper, R. C., and Luzio, J. P. (2007). Ubiquitin-dependent sorting of integral membrane proteins for degradation in lysosomes. Curr. Opin. Cell Biol. *19*, 459–465.

Puri, S., Bachert, C., Fimmel, C. J., and Linstedt, A. D. (2002). Cycling of early Golgi proteins via the cell surface and endosomes upon lumenal pH disruption. Traffic *3*, 641–653.

Puthenveedu, M. A., and Linstedt, A. D. (2004) Gene replacement reveals p115/SNARE interactions are essential for Golgi biogenesis. Proc. Natl. Acad. Sci. USA *101*, 1253–1256.

Raiborg, C., Bache, K. G., Mehlum, A., Stang, E., and Stenmark, H. (2001). Hrs regulates clathrin to early endosomes. EMBO J. *20*, 5008–5021.

Rink, J., Ghigo, E., Kalaidzidis, Y., and Zerial, M. (2005). Rab conversion as a mechanism of progression from early to late endosomes. Cell *122*, 735–749.

Risinger, A. L., and Kaiser, C. A. (2008). Different ubiquitin signals act at the plasma membrane and the Golgi to direct GAP1 trafficking. Mol. Biol. Cell *19*, 2962–2972.

Rosenfeld, J. L., Moore, R. H., Zimmer, K. P., Allizar-Foster, E., Dai, W., Zarka, M. N., and Knoll, B. (2001). Lysosome proteins are redistributed during expression of a GTP-hydrolysis-defective rab5a. J. Cell Sci. *114*, 4499–4508.

Roth, J. A., Horbinski, C., Higgins, D., Lein, P., and Garrick, M. D. (2002). Mechanisms of manganese-induced rat pheochromocytoma (PC12) cell death and cell differentiation. Neurotoxicology *23*, 147–157.

Sanchez, J., *et al*. (2006). GABAergic lineage differentiation of AF5 neural progenitor cells in vitro. Cell Tissue Res. *324*, 1–8.

Scott, P. M., Bilodeau, P. S., Zhdankina, O., Winistorfer, S. C., Hauglund, M. J., Allaman, M. M., Kearney, W. R., Robertson, A. D., Boman, A. L., and Piper, R. C. (2004). GGA proteins bind ubiquitin to facilitate sorting at the *trans* Golgi network. Nat. Cell Biol. *6*, 252–259.

Sengupta, D., Trushel, S., Bachert, C., and Linstedt, A. D. (2009). Organelle tethering by a homotypic PDZ interaction underlies formation of the Golgi membrane network. J. Cell Biol. *186*, 41–55.

Stearman, R., Yuan, D. S., Yamaguchi-Iwai, Y., Klausner, R. D., and Dancis, A. (1996). A permease-oxidase complex involved in high-affinity iron uptake in yeast. Science *271*, 1552–1557.

Stenmark, H., Parton, R. G., Steele-Mortimer, O., Lutcke, A., Gruenberg, J., and Zerial, M. (1994). Inhibition of Rab5 GTPase activity stimulates membrane fusion in endocytosis. EMBO J. *13*, 1287–1296.

Sudbrak, R., *et al*. (2000). Hailey-Hailey disease is caused by mutations in *ATP2C1* encoding a novel Ca2+ pump. Hum. Mol. Genet. *9*, 1131–1140.

Tabuchi, M., Yoshimori, T., Yamaguchi, K., Yoshida, T., and Kishi, F. (2000) Human NRamp2/DMT1, which mediates iron transport across endosomal membranes, is localized to late endosomes and lysosomes in HEp-2 cells. J. Biol. Chem. *275*, 22220–22228.

Thyberg, J., and Moskalewski, S. (1999). Role of microtubules in the organization of the Golgi complex. Exp. Cell Res. *246*, 263–279.

Towler, M. C., Prescott, A. R., James, J., Lucocq, J. M., and Ponnambalam, S. (2000). The manganese cation disrupts membrane dynamics along the secretory pathway. Exp. Cell Res. *259*, 167–179.

Vanlandingham, P. A., and Ceresa, B. P. (2009). Rab7 regulates late endocytic trafficking downstream of multivesicular body biogenesis and cargo sequestration. J. Biol. Chem. *284*, 12110–12124.

Vitelli, R., Santillo, M., Lattero, D., Chiariello, M., Bufilco, M., Bruni, C. B., and Bucci, C. (1997) Role of the small GTPase Rab7 in the endocytic pathway. J. Biol. Chem. *272*, 4391–4397.

Volpicelli, L. A., Lah, J. J., and Levey, A. I. (2001). Rab5-dependent trafficking of the m4 muscarinic acetylcholine receptor to the plasma membrane, early endosomes, and multivesicular bodies. J. Biol. Chem. *276*, 47590–47598.

Wright, R. O., Amarasiriwardena, C., Woolf, A. D., Jim, R., and Bellinger, D. C. (2006). Neuropsychological correlates of hair arsenic, manganese, and cadmium levels in school-age children residing near a hazardous waste site. Neurotoxicology *27*, 210–216.

Yadav, S., Puri, S., and Linstedt, A. D. (2008). A primary role for Golgi positioning in directed secretion, cell polarity and wound healing. Mol. Biol. Cell *20*, 1728–1736.

Yoshino, A., Bieler, B. M., Harper, D. C., Cowan, D. A., Sutterwala, S., Gay, D. M., Cole, N. B., McCaffery, J. M., and Marks, M. S. (2003). A role for GRIP domain proteins and/or their ligands in structure and function of the trans Golgi network. J. Cell Sci. *116*, 4441–4454.

Zhao, P., Zhong, W., Ying, X., Yuan, Z., Fu, J., and Zhou, Z. (2008). Manganese chloride-induced G0/G1 and S phase arrest in A549 cells. Toxicology *250*, 39–46.